## AD NUMBER

**AD248184**

## NEW LIMITATION CHANGE

TO

**Approved for public release, distribution unlimited**

FROM

**Distribution authorized to U.S. Gov't. agencies and their contractors; Administrative/Operational use; Oct 1960. Other requests shall be referred to Department of the Air Force, Washington DC.**

## AUTHORITY

**ONR ltr, 28 Jul 1977**

UNCLASSIFIED

AD 248 184



UNCLASSIFIED

# A Torque Magnetometer for Crystalline Anisotropy Measurements







Technical Report 155
Laboratory for Insulation Research
Massachusetts Institute of Technology

October, 1960

# A Torque Magnetometer for Crystalline Anisotropy Measurements

by

Robert P. Hunt

Laboratory for Insulation Research
Massachusetts Institute of Technology
Cambridge, Massachusetts

Contracts: AF 19(604)-5482
Nonr-1841(10)

October, 1960

# A TORQUE MAGNETOMETER FOR CRYSTALLINE ANISOTROPY MEASUREMENTS*

by

Robert P. Hunt

Laboratory for Insulation Research
Massachusetts Institute of Technology
Cambridge, Massachusetts

Abstract: An instrument designed to measure the torque of magnetic samples automatically and continuously as a function of the angle of an applied magnetic field with respect to the sample is described in detail. General operation of the equipment is outlined, and the system is analyzed on the basis of feedback theory. Results of a temperature run on magnetite and yttrium iron garnet are shown, along with a room-temperature determination of the anisotropy of nickel. Measurements have also been made on the induced anisotropy of polycrystalline yttrium iron garnet and associated relaxation phenomena.

Magnetocrystalline anisotropy energy will generally be an important consideration in any detailed study of magnetic materials.[1] This paper describes an instrument which facilitates the rapid determination of the anisotropy energy of magnetic single crystals.

There are three basic means by which the anisotropy may be experimentally determined. The first is an energy evaluation from the magnetization curves taken with the field at various directions to the crystalline axes. This

---

* Based on a thesis submitted in partial fulfillment of the requirements for the Degree of Master of Science in Electrical Engineering at the Massachusetts Institute of Technology.

1) R. M. Bozorth, "Ferromagnetism," D. Van Nostrand Co., New York, 1955.

is a lengthy and tedious procedure. The second is based on ferromagnetic resonance experiments.[2] This method cannot be used on materials exhibiting a skin effect; also the anisotropy of some materials may have an appreciable frequency dependence.

The final method makes use of the directional dependence of the anisotropy energy to generate a torque which can be measured by a torsion balance. Here the anisotropy is determined under static conditions, but again the procedure is lengthy. To overcome this difficulty we have designed a torque magnetometer that measures the crystalline torque automatically and continuously as a function of the direction of the applied field.

The instrument is capable of measuring torques from 5 to 20,000 dyne-cm over several ranges with a full-scale accuracy of 2%. The torque is plotted on the Y axis of an X-Y recorder. The X axis plots the angle of the applied field, which may be rotated about the crystal. Low torque measurements are somewhat hampered by background vibrations. An entire torque curve may be taken in about one minute. Equipment for controlling temperatures from liquid-nitrogen to 400°C is provided.

## The Torque Magnetometer

### Description of Equipment

The instrument is basically a self-balancing torsion balance which substitutes an electronic feedback system for the torsion fiber. The essentials of the unit are shown in Fig. 1.

The field applied to the crystal is derived from a Varian six-inch magnet, mounted on a gun-sight mount, so that the field may be rotated about a central axis at the midpoint of the magnet's gap. A ten-turn potentiometer ganged to the magnet provides the electrical indication of the magnet's position, which drives the

---

2) L. R. Bickford, Phys. Rev. 76, 137 (1949); 78, 449 (1950).

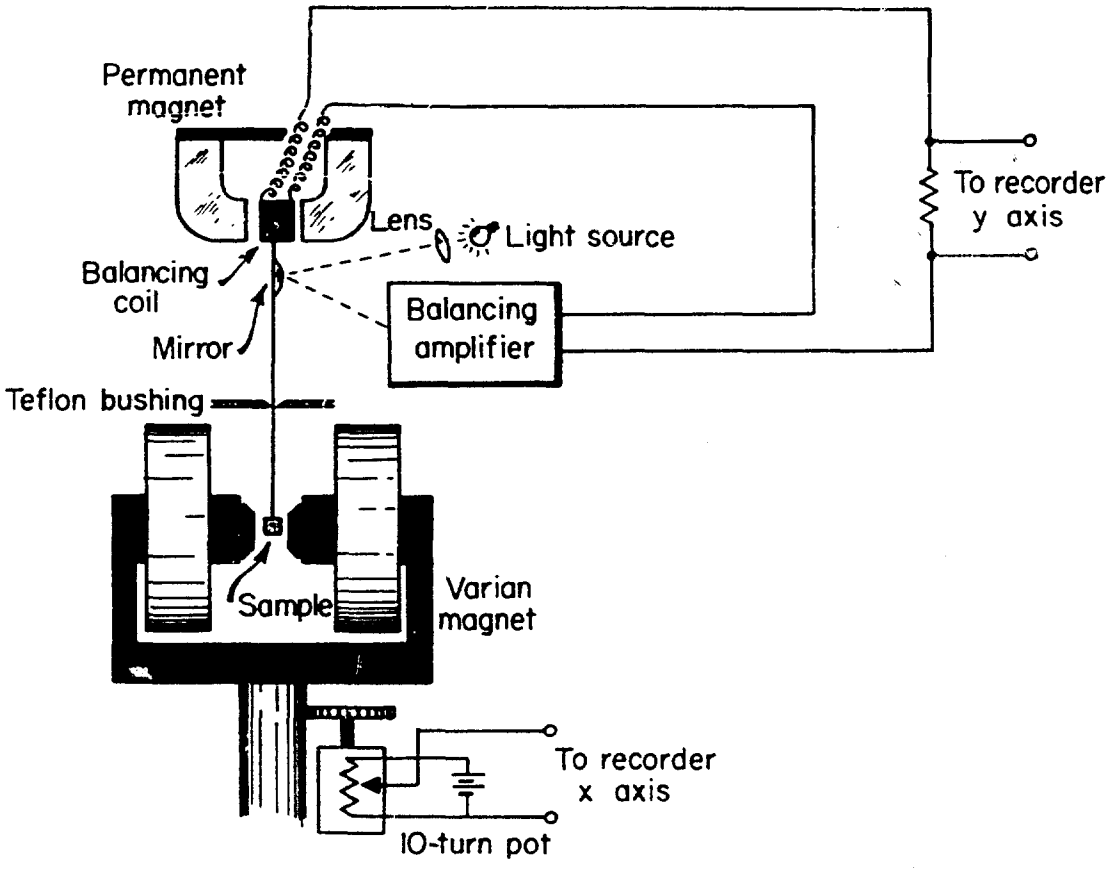


Fig. 1. Torque magnetometer.

X axis of an X-Y recorder.

The sample is placed at the midpoint of the air gap and is suspended by a shaft, on the upper end of which is attached a d'Arsonval type coil assembly, similar to that described by Penoyer,[3] which is situated between the poles of a small magnetron magnet (Fig. 2). The coil and suspension mechanism pivot on a jewel bearing; the shaft is guided by a Teflon knife-edge bushing to reduce friction.

Below the coil assembly a small galvanometer mirror is fixed to the shaft. A stationary light source focuses its beam on the mirror and is reflected onto the cathodes of a dual phototube, which is incorporated in the balancing

3) R. F. Penoyer, "An Automatic Torque Balance," IBM Technical Publication, IBM Corp., Poughkeepsie, New York, 1957.

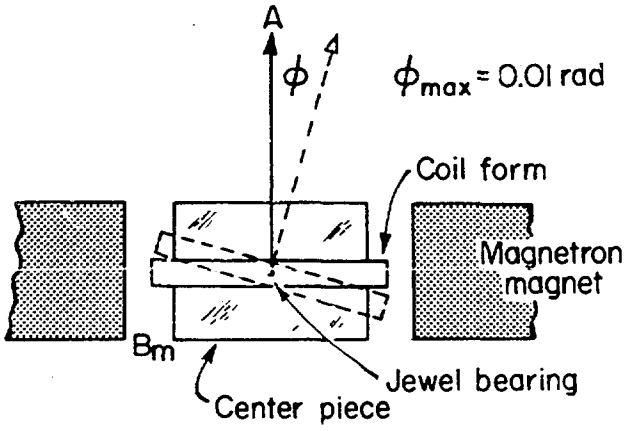


Fig. 2.

Top view of coil assembly.

amplifier. The beam is so adjusted that normally an equal portion of light flux falls on each cathode.

When a torque is applied to the sample shaft, the beam is displaced to one side of the phototube. The latter "senses" the displacement of the shaft and produces an error voltage proportional in magnitude and sign to the displacement. The amplifier converts the error signal to a d-c restoring current which is fed to the balancing coil. The torque developed by the balancing coil is equal but opposite to the applied torque of the crystal. A direct measure of this applied torque is the current, which is then plotted on the Y axis of the X-Y recorder. The entire system is a closed-loop, self-balancing, feedback-controlled unit.

With this apparatus the torque exerted by a crystal sample versus the angle of the applied field can be plotted easily and quickly (cf. Fig. 19, p. 28). The angle of the field may be readily related to the crystallographic axes, which are assumed to be known a priori.*

## Design Criteria

Anisotropy measurements are generally made on single-crystal disks of about 1 cm or less or on small spherical samples of a few millimeters diameter, cemented to the end of the sample shaft. Care must be taken to avoid attaching

* Orientation is determined by X rays prior to experiment.

the sample so rigidly (as with a spring-loaded clamp) that the crystal is under a strain since this would affect the anisotropy behavior.[4] The field gap of the Varian magnet is two inches, allowing plenty of room for a Dewar or heating furnace.

A survey of the materials that had been previously measured indicated that the torque magnetometer should be capable of measuring torques from a few up to about $10^4$ dyne-cm. Together with a knowledge of the amplifier-current output and the magnetron magnet's field $B_m$, this provides the information necessary for the design of the balance coil. The Varian magnet must be capable of saturating the crystal in question to avoid analytical complications.

Since the device is a feedback system, the frequency response must be considered. It clearly must be flat over the region of interest. This region may be determined from the field-angle dependence of the torque and the angular velocity of rotation of the magnet.

Bozorth[5] showed that the most "rapid" significant variation of torque for the cubic and hexagonal structure has a $6\theta$ dependence. Hence we will assume this to be our highest-order effect. $\theta$ is determined by the angular velocity of the field, $\omega_m$, i.e.,

$$\theta = \omega_m t, \tag{1}$$

where $\omega_m \leqslant 2\pi/15$ radians/sec and is limited by the magnet's drive motor. Hence, the maximum radian frequency to be encountered is $6\omega_m$ or $12\pi/15$ radians/sec, and the unit must be linear up to this value.

---

4) D. Gugan and G. Rowlands, Proc. Phys. Soc. (London) 72, 207 (1958).

5) R. M. Bozorth, Phys. Rev. 50, 1076 (1936).

## System Analysis

### Block-Diagram Representation

From Fig. 1 and the description of the equipment, a general block diagram (Fig. 3) may be formed for the system. For convenience we shall work

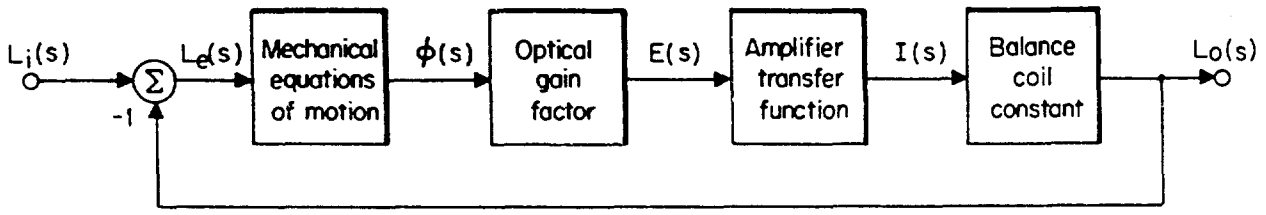


Fig. 3. General block diagram.

mainly in the frequency domain making use of the Laplace transform theory.[6] $L_i(s)$ is defined as the Laplace transform of the input torque function; $L_e(s)$ is an error torque given by the difference between input torque $L_i(s)$ and output torque $L_o(s)$. This error torque acts on the shaft to produce a small angular deflection $\phi(s)$ which generates, through the optical system and phototube sensor, an error voltage $E(s)$. $E(s)$ is converted by the amplifier to a current $I(s)$, which in turn produces the output torque $L_o(s)$ through the balance coil. In each case the parameters may be inversely transformed to find the corresponding time-domain function; i.e., $L_i(s) \leftrightarrow L_i(t)$, etc.

We now must formulate the transfer function for the various blocks.

### Mechanical Equation

The only mechanical equation is that which governs the shaft motion. If

---

6) J. A. Aseltine, "Transformation Methods in Linear System Analysis," McGraw-Hill Book Co., New York, 1958.

J is the moment of inertia* of the shaft, $\alpha$ the damping factor, and K the spring constant, and if $\phi$ is the angle of the balance coil's area vector with the faces of the magnetron magnet's pole pieces (Fig. 2), we may write Newton's law for the shaft as

$$J \frac{d^2\phi}{dt^2} + \alpha \frac{d\phi}{dt} + K\phi = L_i(t) + L_f - L_o(t). \tag{2}$$

The frictional torque $L_f$ was found to be $10^{-7}$ newton-meters (1 dyne-cm) and may be neglected. Thus,

$$J \frac{d^2\phi}{dt^2} + \alpha \frac{d\phi}{dt} + K\phi = L_i - L_o. \tag{3}$$

Transforming to the frequency domain and assuming that for initial conditions $\phi(0) = 0$ and $\phi'(0) = 0$, we get

$$Js^2\phi(s) + \alpha s\phi(s) + K\phi(s) = L_i(s) - L_o(s). \tag{4}$$

Solution for $\phi(s)$ gives a relation between error torque and angular deflection:

$$\phi(s) = \frac{L_i(s) - L_o(s)}{Js^2 + \alpha s + K} = \frac{L_e(s)}{Js^2 + \alpha s + K} . \tag{5}$$

The shaft is a long, hollow brass rod, having a moment of inertia given by

$$J = \frac{1}{2} m (R_1^2 + R_2^2) , \tag{6}$$

where m is the mass, and $R_1$ and $R_2$ the inner and outer radii, respectively.

The damping factor $\alpha$ arises partly from friction and windage which cannot be calculated, but principally from the action of the balance-coil form, which is a rectangular brass loop and acts as a shorted turn in the field $B_m$ of the magnetron magnet. The spring constant K comes primarily from the torsion of the wire leads connected to the balance coil and is small but not negligible.

---

* In the system analysis we shall use mks rationalized units. Some of the cgs units will be indicated for reference.

## Optical Gain Factor

The optical gain factor is defined as the output voltage of the sensing unit per radian of angle rotated by the shaft:

$$\text{optical gain} = K_1 = \frac{\Delta E(t)}{\Delta \phi} = \text{constant.} \tag{7}$$

A linear variation of $E(t)$ with $\phi$ is based on the assumption that the output current of a phototube is an approximately linear function of the amount of flux falling on its cathode. As $\phi$ varies linearly, the light flux on one section of the dual phototube increases while that on the other decreases linearly. This assumption was verified by experiment. Hence,

$$\begin{aligned} E(t) &= K_1 \phi(t), \\ E(s) &= K_1 \phi(s). \end{aligned} \tag{8}$$

$E(t)$ is physically the output of the difference-amplifier circuit (Fig. 4).

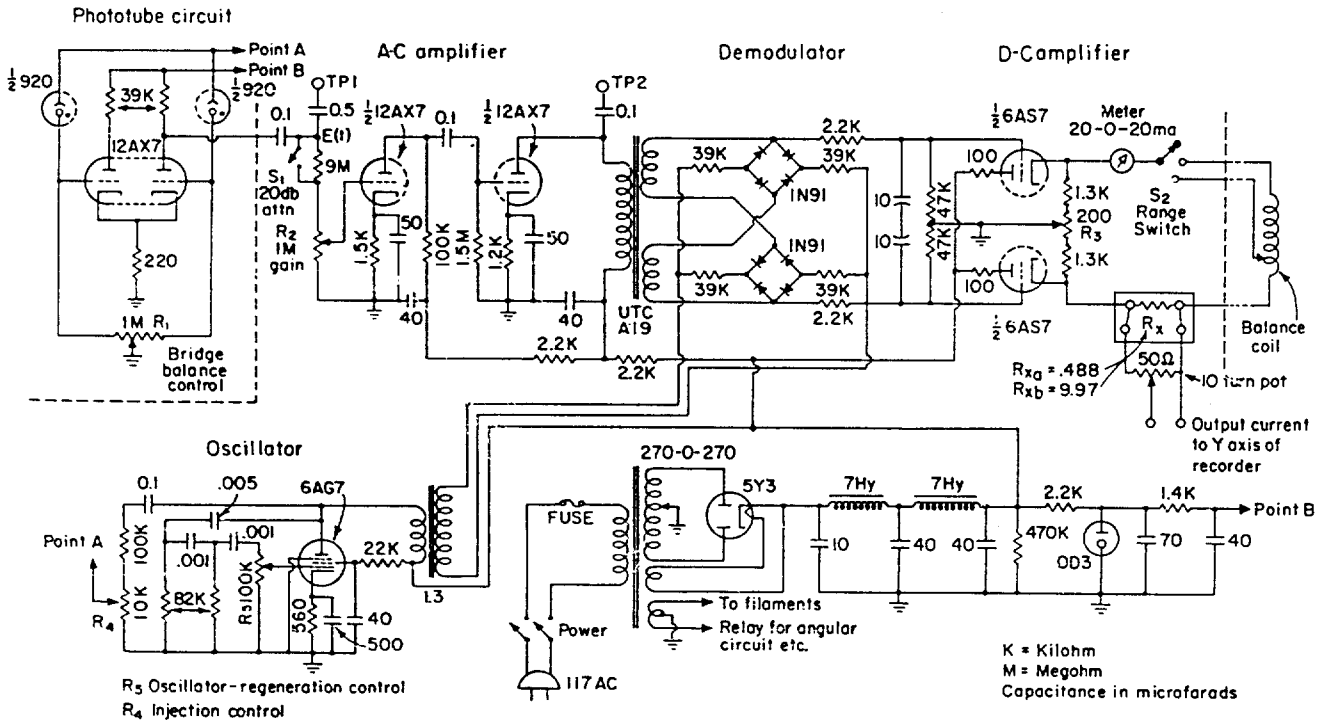


Fig. 4. Circuit diagram.

The dual phototube forms a bridge circuit along with the variable 1-megohm resistor $R_1$. A 3-volt 400-cycle signal is applied across the phototube.* When $\phi = 0$, an equal light flux falls on each section, and each tube has the same current. The signals at both grids of the 12AX7 difference amplifier are equal, and the difference-amplifier output is zero. As $\phi$ deviates from 0, a misbalance in the bridge occurs, and the output voltage E(t) is a measure of the difference between the grid signals and hence of $\phi$. E(t) is a 400-cycle signal whose magnitude is proportional to $\phi$. The phase of E(t) (or its sign) is 0 degrees for $\phi > 0$ and 180 degrees for $\phi < 0$. Another approach is to think of the phototube circuit as a chopper system acting at a 400-cycle rate.

The steps used in arriving at Eqs. 8 are shown diagrammatically in Fig. 5. In Fig. 5a, E(t) is related to $\phi$ through the various constants of the phototube and the difference-amplifier gain. The constants may be lumped into a single optical-gain parameter $K_1$ in the expression for E(t). In Fig. 5b, the the sine multiplier is dropped, since it is effectively canceled out in the demodulator circuit, as will be shown.

Amplifier

Since E(t) is a 400-cycle signal modulated with the essential information about $\phi$, it may be amplified by conventional a-c means. This is the function of the second 12AX7 in Fig. 4. The signal is then passed through a transformer to a phase-sensitive detector where the 400-cycle signal is demodulated. After detection it is transmitted through a filter to the grids of a 6AS7 acting as a current amplifier; the balance coil is connected across the cathodes of this tube. The 6AG7 is merely an oscillator that provides the 400-cycle chopping and detecting voltage.

---

* The phototubes rectify the current, giving half-wave pulses. This does not affect the above analysis.

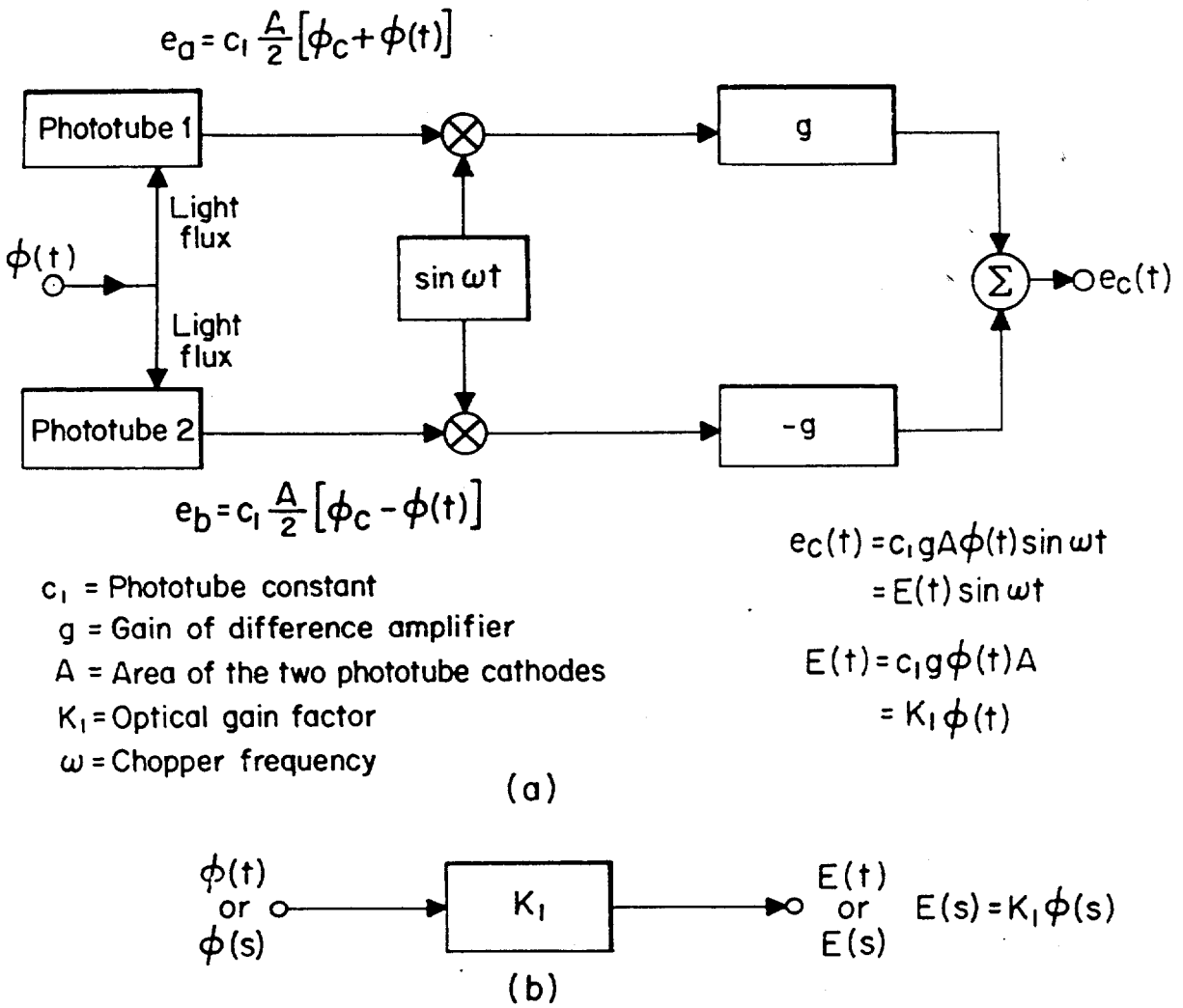


Fig. 5. Phototube circuit operation: (a) functional diagram, (b) equivalent representation.

For a static deflection $\phi_o$ of the shaft, the output of the phase-sensitive detector is a d-c voltage whose magnitude is a measure of $\phi_o$. If the voltage is greater than 0, $\phi_o > 0$, and vice versa.

In the frequency domain a transfer-conductance function F(s) for the amplifier-demodulator-current amplifier system is defined as

$$F(s) = \frac{I(s)}{E(s)} = \frac{\text{output current}}{\text{input voltage}} . \qquad (9)$$

The a-c amplifier, since it operates at 400 cycles, provides no other contribution to F(s) than a straight frequency-independent gain multiplier.

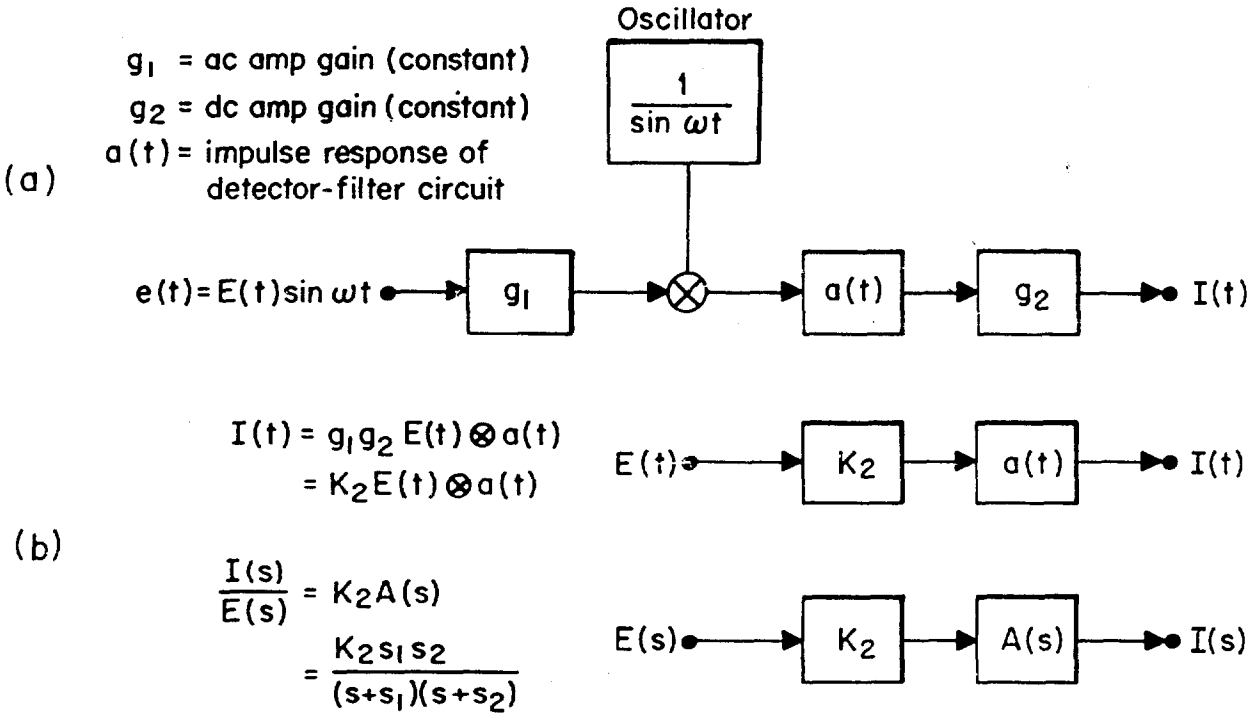


Fig. 6. Amplifier detector: (a) operation, (b) reduced diagram.

Similarly, there are no reactive elements in the d-c current amplifier. Hence, any poles or zeros for the unit must originate in the detector circuit.

The operation of the amplifier is shown schematically in Fig. 6. In Fig. 6b, the $1/\sin \omega t$ multiplier has been omitted since it is effectively canceled by the corresponding multiplier in the phototube circuit. The various tube gain factors have been concentrated in the single gain factor $K_2$. The symbol a(t) represents the impulse response of the filter and detector circuit, and I(t) is related to E(t) in the time domain by the convolution of $K_2 a(t)$ with E(t), i.e.,

$$I(t) = K_2 a(t) \otimes E(t) \triangleq K_2 \int_0^\infty a(\tau) E(t - \tau) d\tau \ . \qquad (9)$$

The frequency-domain equivalence of this is given in Fig. 6b, where $a(t) \leftrightarrow A(s)$, and A(s) is determined by the filter and detector circuits. It is noted that

$$I(t) \leftrightarrow I(s) = K_2 \mathcal{L} \int_0^\infty a(\tau) E(t - \tau) d\tau = K_2 A(s) E(s) \ . \qquad (10)$$

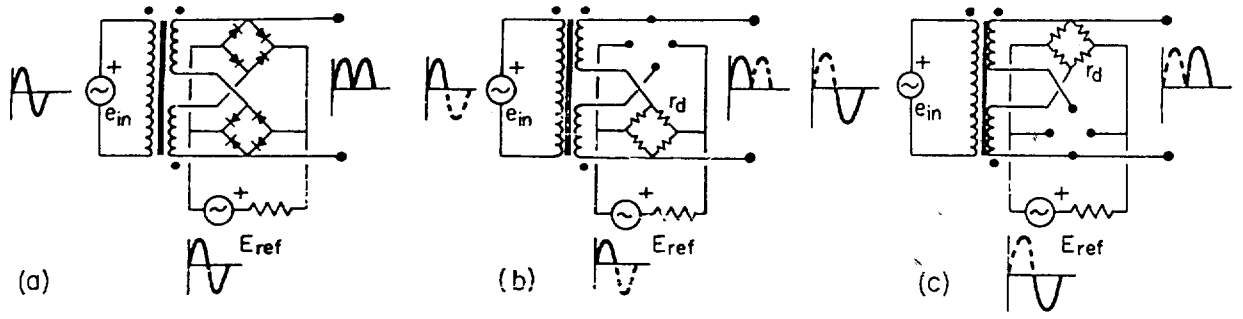


Fig. 7. Detector-circuit operation: (a) complete cycle, (b) first half-cycle, (c) second half-cycle.

The principal elements of the detector circuit are: the coupling transformer, the diodes, and the filter circuit. The diodes switch the filter from one section of the transformer secondary to the other on alternate half-cycles. This is clarified in Fig. 7, where $E_{ref}$ is a large 400-cycle reference signal that sweeps the diodes of each ring alternately open and closed on each half-cycle. To the filter circuit the diodes appear as a small resistance (effectively the forward resistance of a single diode in series with the transformer secondary). For analytical purposes the circuit may be simplified to that of Fig. 8, where E is the Thevenin equivalent voltage output of the transformer, $r_t$ the secondary resistance (one section), $L_t$ the secondary inductance, $r_d$ the diode forward resistance, R an exterior resistor (4400 ohms), C the filter capacitance, and $R_g$ the grid resistor of the 6AS7. Actually $r_d$ is so small and $R_g$ so large that both may be dropped from consideration. The circuit of Fig. 9 represents an adequate approximation to the detector-filter circuit. This is a simple R-L-C series circuit which has the transfer function

$$\frac{e_o(s)}{e(s)} = \frac{c}{s^2 + \frac{(R + r_t)s}{L_t} + \frac{1}{L_t C}}, \qquad (11)$$

where c is a constant multiplier. The roots of the denominator of Eq. 11 turn

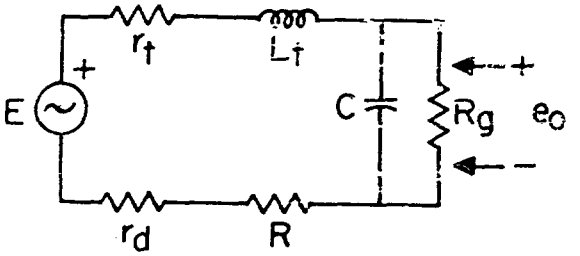


Fig. 8.

Equivalent detector circuit.

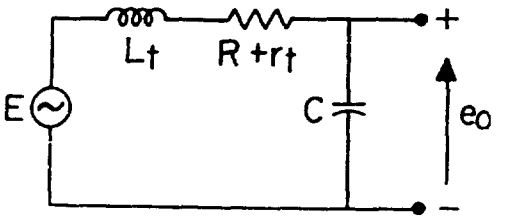


Fig. 9.

Reduced detector circuit.

out to be real:

$$\frac{e_o(s)}{e(s)} = \frac{c}{(s + s_1)(s + s_2)}; \tag{12}$$

$$s_{1,2} = \frac{(R + r_t)}{2L_t} \pm \sqrt{\frac{(R + r_t)^2}{(2L_t)^2} - \frac{1}{L_t C}}. \tag{13}$$

Equation 12 expresses the frequency-dependent function that describes the amplifier. For convenience, Eq. 12 may be put into the form

$$F(s) = \frac{K_2 s_1 s_2}{(s + s_1)(s + s_2)}, \tag{14}$$

$$F(0) = K_2, \tag{15}$$

where F(s) becomes a single constant gain $K_2$ for s = 0 (i.e., $K_2$ is defined as the static gain).

## Balance-Coil Constant

The final stage of the system is the conversion of the output current of the amplifier to a torque. This is accomplished by the balance coil located between the poles of the magnetron magnet. The torque of a coil of moment m in a magnetic field is

$$\bar{L} = -\bar{m} \times \bar{B}. \tag{16}$$

For our geometry and parameters (cf. Fig. 2),

$$L = -mB_m \cos \phi \cong -mB_m, \tag{17}$$

if a steady torque is assumed. For a flat coil with n turns and area A the moment is given by

$$m = nAI, \tag{18}$$

where I is the current. The area A, as before, is roughly the area of the pole pieces whose radii are r. Therefore the torque becomes

$$L = -n\pi r^2 IB_m = -K_3 I, \tag{19}$$

where $K_3$ is defined as the balance-coil constant. The torque output is mechanically coupled to the shaft, thus completing the feedback loop. The proper sign of $K_3$ is obtained by correct polarity of the coil leads to produce a negative feedback torque. The balance coil has two taps, one at n = 10 and one at n = 100, for control over the system sensitivity.

## The Entire System

The block diagrams for the entire system now become those of Fig. 10. Table 1 summarizes the various relationships thus far derived. The parameters on the right must be found experimentally (cf. next section): in addition, several of the constants (for example $\alpha$, $K_3$, and $s_{1,2}$) were measured separately to ensure accuracy.

Table 1. Review of parameters.

| | |
|---|---|
| $J = \frac{1}{2} m(R_1^2 + R_2^2)$<br>$\triangleq$ moment of inertia<br>$a \triangleq$ mechanical damping term | $m$ = mass of shaft<br>$R_1$ = inner radius of shaft<br>$R_2$ = outer radius of shaft |
| $s_{1,2} = \frac{(R + r_t)}{2L_t} \pm \sqrt{\frac{(R + r_t)^2}{4L_t^2} - \frac{1}{L_t C}}$<br>= amplifier poles | $R$ = 4400-ohm resistor<br>$r_t$ = transformer resistance<br>$L_t$ = transformer inductance<br>$C$ = filter capacitance |
| $K_3^* = n\pi r^2 B_m$<br>$\triangleq \frac{L_o}{I}$ | $n$ = number of turns on coil<br>$r$ = radius of pole pieces of magnetron magnet<br>$B_m$ = field of magnetron magnet |
| $\frac{\phi(s)}{L_e(s)} = \frac{1}{Js^2 + as + K}$ | $K$ = shaft spring constant |
| $F(s) = \frac{K_2 s_1 s_2}{(s + s_1)(s + s_2)}$<br>$\triangleq \frac{I(s)}{E(s)}$ | $K_3$ = static amplifier gain constant |
| $\frac{E(s)}{\phi(s)} = K_1$<br>$\triangleq$ optical gain constant | |
| *The negative sign appearing in Eq. 19 has been put into the feedback loop to convene with standard notation. | |

To analyze the complete system,[7] the following conventional definitions are made:

7) F. L. Nixon, "Principles of Automatic Controls," Prentice-Hall, New York, 1953.

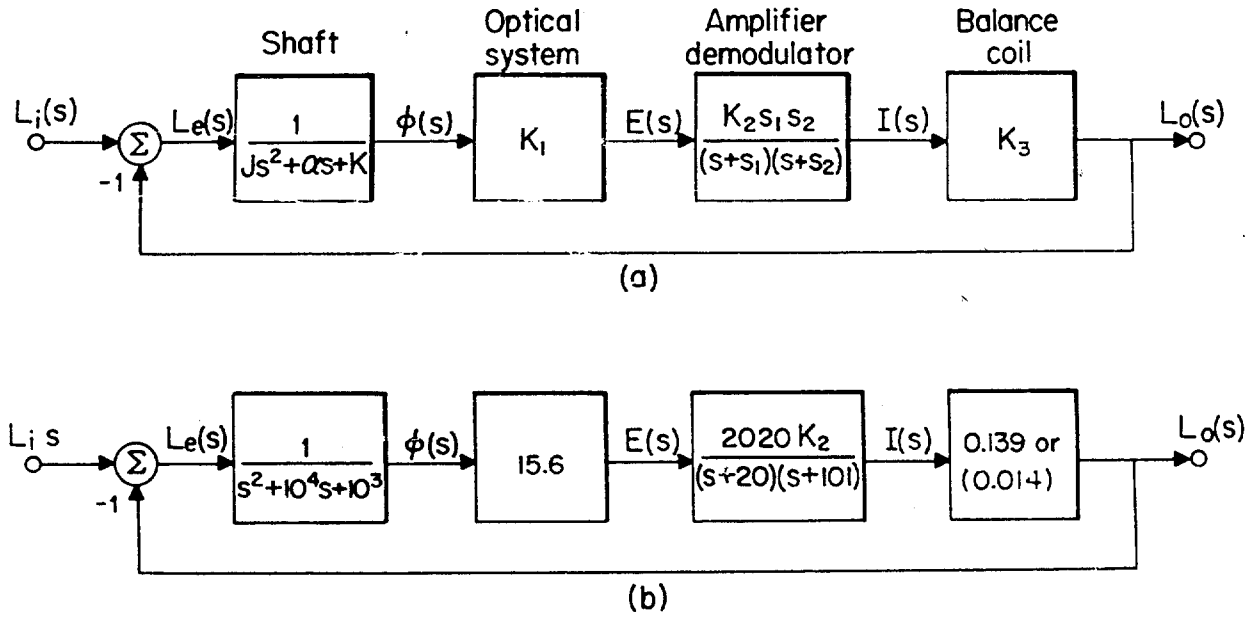


Fig. 10. Block diagram: (a) general, (b) numerical.

$$G(s) = \frac{L_o(s)}{L_i(s)} = \text{open-loop transfer function (with no feedback)}$$

$$W(s) = \frac{L_o(s)}{L_i(s)} = \text{closed-loop transfer function (with feedback)}$$

The loop may be physically severed by disconnecting the balance-coil leads and substituting a load resistor for the coil. The current flowing in this load resistor, multiplied by $K_3$, gives the effective open-loop output torque.

From the block diagram of Fig. 10 we find that

$$G(s) = \frac{K_1 K_2 K_3 s_1 s_2}{(Js^2 + \alpha s + K)(s + s_1)(s + s_2)} . \qquad (20)$$

The static gain of the amplifier, $K_2$, may be varied at will through the gain control $R_2$ of Fig. 4. The balance-coil constant $K_3$ similarly is double-valued at will. We assume operation on the tap at n = 100. The remaining parameters of Eq. 20 are all constants. At the sacrifice of generality we now substitute numerical values for all parameters except $K_2$, to permit a number of simplifications that will ultimately yield a relatively simple expression governing the

Table 2. Various numerical values.

| Quantity | Symbol | Value |
|---|---|---|
| Mass of shaft | m | $3.8 \times 10^{-2}$ kg |
| Inner radius of shaft | $R_1$ | $2.0 \times 10^{-3}$ m |
| Outer radius of shaft | $R_2$ | $2.5 \times 10^{-3}$ m |
| Radius of magnetron-magnet pole pieces | r | $2.54 \times 10^{-2}$ m |
| Magnetron-magnet field | $B_m$ | 0.85 weber/$m^2$ |
| Transformer inductance | $L_t$ | 100 hy |
| Transformer resistance | $r_t$ | 7700 ohms |
| Total equivalent detector resistance | R | 12,100 ohms |
| Optical gain | $K_1$ | 15.6 volts/radian |
| Static gain of amp | $K_2$ | variable |
| Torque constant | $K_3$ | 0.139 n-m/amp<br>0.014 n-m/amp |
| Amplifier poles | $s_1$<br>$s_2$ | 20/sec<br>101/sec |
| Moment of inertia | J | $2 \times 10^{-7}$ kg-$m^2$ |
| Damping factor | a | $2 \times 10^{-3}$ n-m-sec/radian |
| Spring constant | K | $2 \times 10^{-4}$ n-m/radian |
| Number of coil turns | n | 100 or 10 |

behavior of the apparatus over the frequency range of interest.

Table 2 lists the various numerical values. Substituting these into Eq. 20, we get

$$G(s) = \frac{2.2 \times 10^{10} K_2}{(s + 0.1)(s + 10^4)(s + 20)(s + 101)} . \qquad (21)$$

We have shown (cf. p. 5) that the maximum operating frequency is about 0.4 cps ($\cong$ 2.5 radians/sec). Measurements showed responses up to radian frequencies of about 50. Hence, we may neglect the pole at $s = -10^4$. G(s) may be approximated by

$$G(s) \cong \frac{2.2 \times 10^6 K_2}{(s + 0.1)(s + 20)(s + 101)} . \qquad (22)$$

Now, W(s) may be evaluated

$$W(s) = \frac{G(s)}{1 + G(s)} \cong \frac{2.2 \times 10^6 K_2}{s^3 + 121s^2 + 2032s + 2.2 \times 10^6 K_2} \quad . \tag{23}$$

It is also instructive at this point to substitute the usual value for $K_2$, 0.077 mho,

$$W(s) = \frac{1.7 \times 10^5}{(s + 116)(s + 2.5 + j38)(s + 2.5 - j38)} \quad . \tag{24}$$

Further, if we neglect the pole at s = -116 (this is not entirely valid at frequencies around 50 but useful nevertheless), we get

$$W(s) = \frac{1.5 \times 10^3}{(s + 2.5 + j38)(s + 2.5 - j38)}$$

$$= \frac{k}{(s + a_d + j\omega_o)(s + a_d - j\omega_o)} \quad , \tag{25}$$

where $a_d$ is a damping term for the response and $\omega_o$ its natural resonant frequency.

## Experimental Verification

### Determination of Parameters

The numerical values of the parameters of Table 1 appear in Table 2. The torque constant $K_3$ was evaluated by several different experimental procedures to ensure accuracy, because calibration of the instrument depends on this value.

The optical and static amplifier gain parameters were determined by deflecting the shaft by a given angle and measuring E and I. In this way Figs. 11 and 12 were obtained.

The expression for F(s) of Eq. 14 becomes

$$F(s) = \frac{2020 K_2}{(s + 20)(s + 101)} \quad , \tag{26}$$

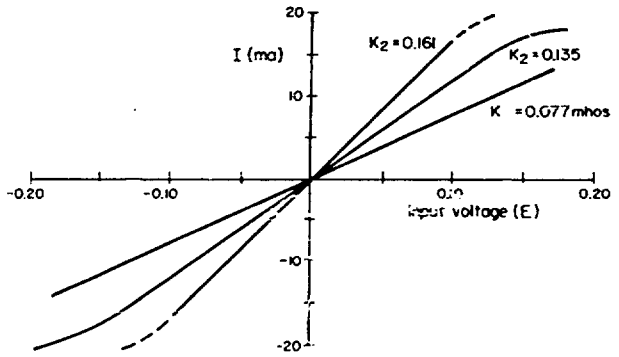


Fig. 11.
Optical gain characteristic.

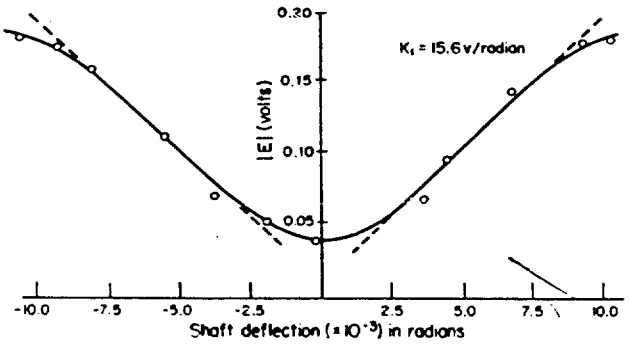


Fig. 12.
Static gain function.

as verified in part by a frequency-response curve of the amplifier. The response curve of Fig. 13 shows the break point at s = j20; that at s = j101 was beyond measurement.

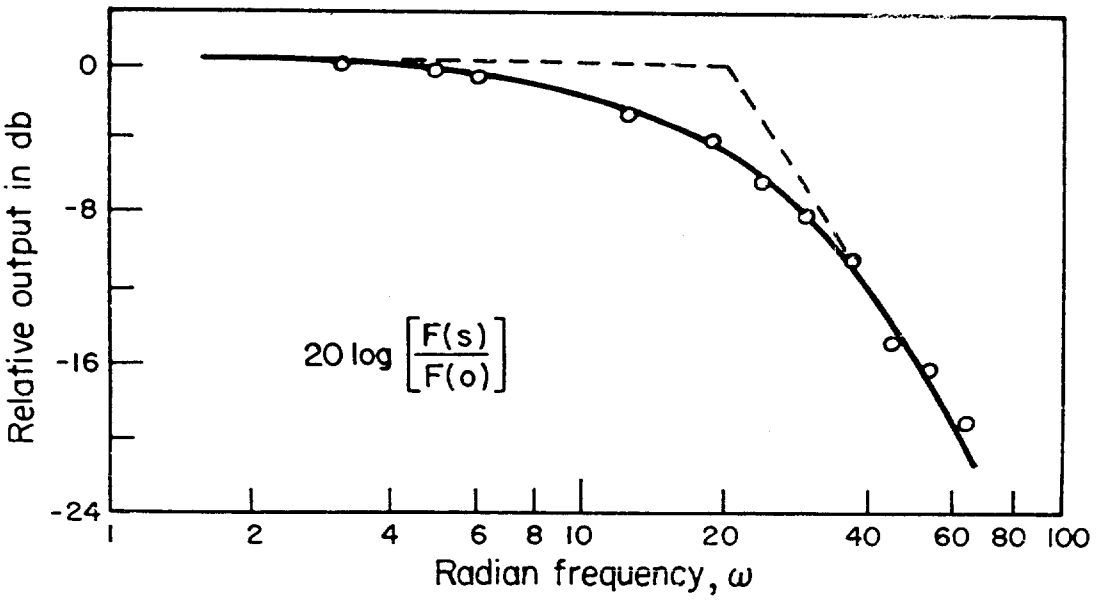


Fig. 13. Amplifier-response curve.

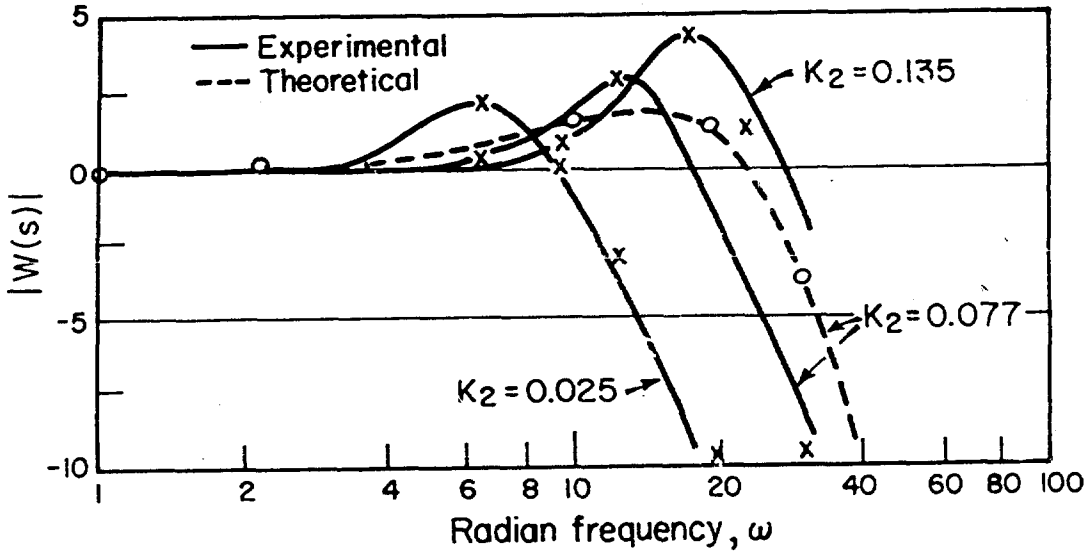


Fig. 14. Closed-loop gain response.

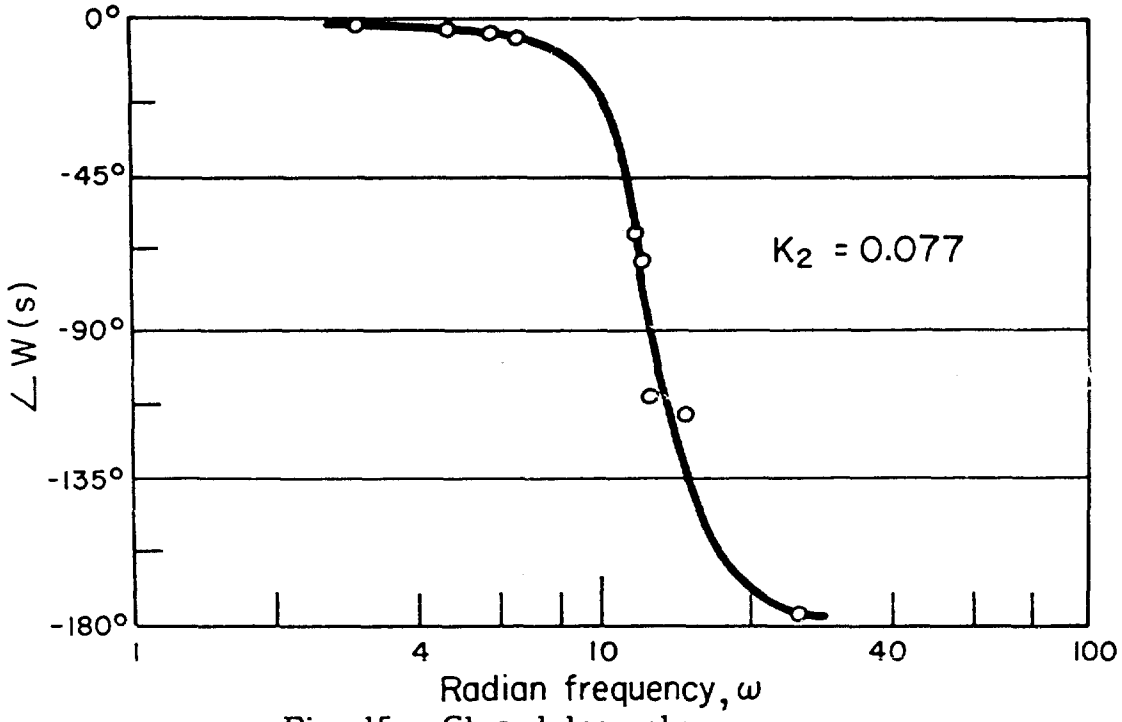


Fig. 15. Closed-loop phase response.

Bode Diagram

To verify the closed-loop operation, a Bode gain magnitude and a phase diagram were taken for various amplifier gain settings $K_2$ as shown in Figs. 14 and 15, along with a theoretical curve for $K_2 = 0.077$. The general character

of the curves agrees with that predicted in that the system is representable by a pair of complex conjugate poles (cf. Eq. 25). The measured resonant frequency is about 14, as compared to 38 predicted by Eq. 25. The measured phase diagram shows the expected rapid transition from around 0 to -180 degrees at the resonance point.

To get the experimental Bode plots, a circular coil was suspended from the shaft in the field of the Varian magnet and excited by a sinusoidal current source. The presence of this coil substantially altered the parameters of the system, causing disagreement with the results of Eq. 24. In particular the coil increased the mechanical damping factor of electromagnetic origin from $2 \times 10^{-3}$ to $9 \times 10^{-3}$ n-m-sec. Substituting this new value of $a$ into Eq. 20 and evaluating the new closed-loop response function shows that a resonant frequency of 19.5 radian/sec and a system damping factor of 7.9 are achieved for the system. A plot of the revised function W(s) in Fig. 14 shows good agreement with the experimental results. The increase in the mass of the shaft and the equivalent spring constant prove of negligible importance.

Transient Analysis

The transient response of the unit was measured by applying a step of torque to shaft (by brushing the shaft with a finger) and observing the subsequent behavior for different gains. The system demonstrated an exponentially damped oscillatory response. The step response (for a unit step) may be found from Eq. 25. A unit step has the Laplace transform 1/s. The output in the frequency domain is then

$$L_o(s) = \frac{W(s)}{s} = \frac{k}{s(s + a_d + j\omega_o)(s + a_d - j\omega_o)} . \qquad (27)$$

The output response may be inversely transformed as

$$L_o(t) = \frac{k}{(a_d^2 + \omega_o^2)} \left[ 1 - e^{-a_d t} \left( \frac{a_d \sin \omega_o t + \omega_o \cos \omega_o t}{\omega_o} \right) \right] . \qquad (28)$$

Since $a_d \ll \omega_o$, Eq. 28 simplifies to

$$L_o(t) = \frac{k}{\omega_o^2}(1 - e^{-a_d t} \cos \omega_o t) = (1 - e^{-2.5t} \cos 38t), \qquad (29)$$

where $k = 1.5 \times 10^3$ (cf. Eq. 25). Note that for $t \gg 1/2.5$, $L_o \rightarrow 1$, as expected.

The step response was plotted with a Sanborn time-base recorder. From the transient curves the following values were found:

| $K_2$ | $\omega_o$ | $a_d$ | |
|---|---|---|---|
| 0.077 | 26.4 | 1.53 | Measured |
| 0.135 | 31.4 | 0.82 | |
| 0.147 | 34.5 | 0.32 | |
| 0.160 | 37.7 | 0.00 | |
| 0.077 | 38.0 | 2.50 | Calculated |

Again reasonable agreement is observed between theory and experiment for $K_2 = 0.077$. The values of $a_d$ and $\omega_o$ are, of course, dependent on the gain setting. For some critical gain setting, $a_d < 0$, and the system goes into an unstable condition of oscillation. This occurred for a gain of $K_2 = 0.160$.

## Open-Loop Considerations

No open-loop data could be taken because inherent open-loop drift in the output stage of the amplifier would rapidly drive the system into a nonlinear region of operation, as shown by the fact that the open-loop system function (cf. Eq. 22) has a pole very close to zero and hence a very large open-loop gain for low frequencies.

## Stability Considerations

An exaggerated Nyquist diagram of $G(s)/K_2$ (Eq. 22) is shown in Fig. 16. The Nyquist criterion[8] states that for stability

8) C. Newton, L.A. Gould, J. F. Kaiser, "Analytical Design of Linear Feedback Controls," John Wiley and Son, New York, 1957, p. 302.

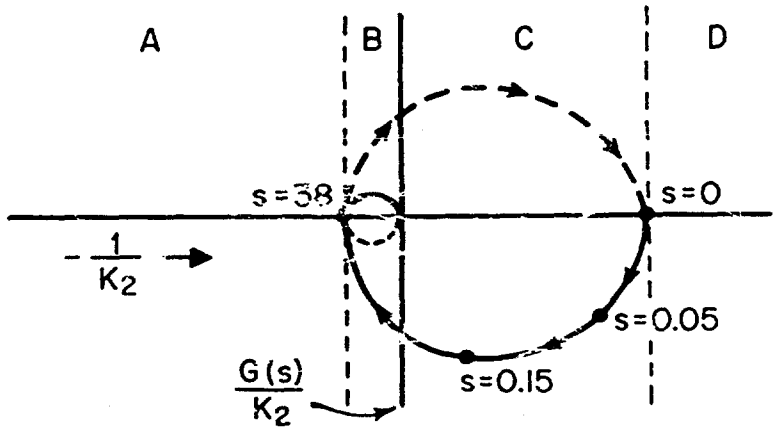


Fig. 16.

Nyquist plot.

$$Z = N + P = 0, \tag{30}$$

where Z is the number of right-hand plane poles in W(s), N the net number of positive encirclements around a $-1/K_2$ point in the Nyquist polar plot of $G(s)/K_2$,* and P the number of right-hand plane poles of G(s). Clearly from Eq. 22, P = 0. The Nyquist diagram is broken into four distinct regions. For region A there are no encirclements of the $-1/K_2$ point; hence, N = 0 and Z = N + P = 0. Here the system must be stable where $0 \leqslant K_2 < 0.11 = 1/9.2$. For region B, N = -2 and thus the system is unstable according to Eq. 30. For region C, N = -1 and again instability exists. For region D, N = 0; hence Z = 0 and stability is again implied. This corresponds to $-1/K_2 \geqslant 1.1 \times 10^4$. Actually, for any $K_2 < 0$ the system runs into a highly nonlinear region of operation where the coil form bangs against its stops; thus operation at this value has virtually no significance here.

Stability prevails only for values of $-1/K_2$ that lie entirely to the left of the polar plot. In the transient response we found the system to be unstable for $K_2 > 0.16$.

---

*N is positive if the plot is traversed in a counter-clockwise direction for increasing values of $\omega$.

## Operation

### Calibration and Accuracy

In the torque-measuring equipment the important parameters for calibration of the X-Y recorder are the balance-coil constant $K_3$ and the current-measuring resistor $R_x$. The latter (cf. Fig. 4) is simply a small resistance in series with the balance coil. The voltage across $R_x$, when plotted on the recorder, gives the feedback current, which in turn gives the feedback torque from the relation

$$L_o = K_3 I = \frac{K_3 E_r}{R_x}, \tag{31}$$

where $E_r$ is the voltage recorded. $R_x$ may be one of two plug-in resistors. There is also a voltage-dividing potentiometer across $R_x$ to permit a more flexible adjustment of the recorder range. The angular circuit which monitors the angle of the field with respect to the crystal is given in Fig. 17. The Helipot is ganged directly to the Varian magnet and the output voltage is directly proportional to the angle of rotation. The circuit satisfies the proper input

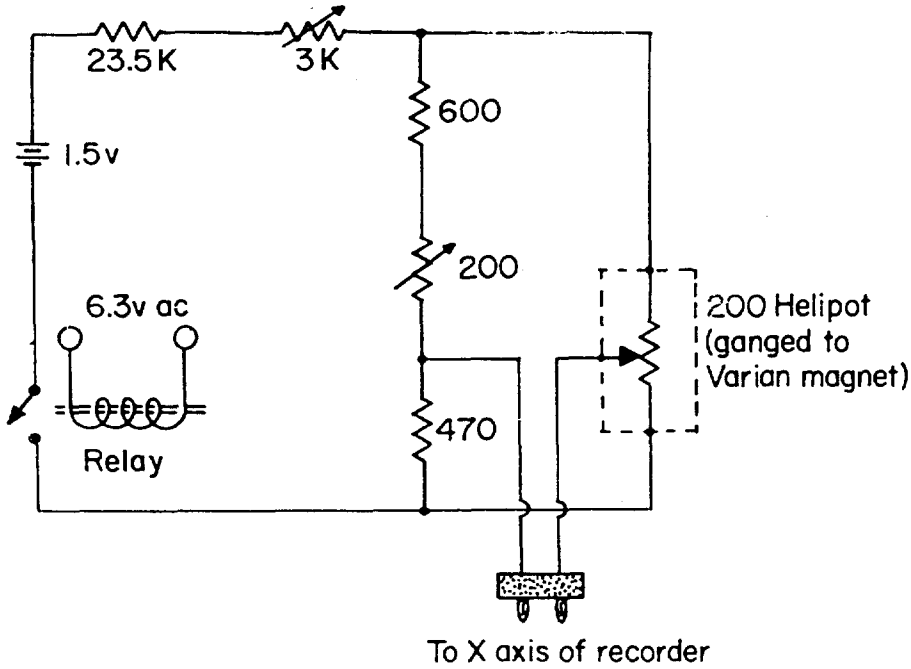


Fig. 17. Angular circuit.

requirements of the recorder's X axis. The two variable resistors permit adjustment of the zero point and compensation for changes in battery voltage. The accuracy of the angular circuit is limited to about $\pm 1\%$ principally by the readability of the recorder. Accuracy for the torque axis is conservatively set at about 2% for torques above 300 dyne-cm. Below this figure, noise and building vibrations present increasing difficulty.

Errors

Several possible sources of error have not yet been fully discussed. The first is a possible interaction between the rotating Varian field and the torque equipment. This condition was found to exist through an interaction of the rotating field with the phototubes,* but was entirely eliminated by magnetic shielding, which also greatly reduced noise pickup.

A second source of error stems from a possible misorientation of the crystal plane on the shaft. X-ray techniques are accurate to only about $\pm 1/2^{\circ}$ with our equipment in aligning a crystalline plane, and extreme care must be used to maintain this tolerance in transferring the crystal from the X-ray apparatus to the magnetometer. This error is approximately proportional to the square of the angular deviation from orientation, to which must be added demagnetization-correction factors if the sample is not ellipsoidal in shape. Hence, information about the second-order anisotropy constant may be completely enshrouded by small errors.

A quite different problem arises if the crystal plane is properly oriented but the surfaces of the crystal are not parallel to this plane. Here a consideration of the demagnetization factors for the altered geometry becomes requisite. It would be expected that at least a $2\theta$-error variation would be obtained for this case.

---

* A computation verified the fact that the magnetic force exerted on the electrons by the Varian's magnetic field was comparable to the electric force exerted by the E field of the phototube.

## Data Analysis

### Basic Method

Our essential approach to data analysis lies in approximating the experimental curve by a Fourier series[9] and equating this to the theoretical torque derived from the anisotropy-energy expansion. In this way a considerable amount of the information contained in the curve is used.

This procedure tacitly assumes that there is negligible effect from the magnetostrictive anisotropy, that the demagnetization energy is isotropic in nature, and that the crystal must be saturated by a field that is large compared to the demagnetizing field, so that the magnetization vector lies in the measuring plane and essentially parallel to the applied field. These assumptions are never precisely attained. First the anisotropy energy prevents the magnetization from lying exactly parallel to the field. Another factor that may influence the magnetization is, for instance, the possible presence of an inhomogeneous demagnetizing field (compared to the applied field) near the edges of a disk-shaped sample. This could influence the torque so as to make the anisotropy constants appear to have a field dependence.[10]

Theoretically, the torque curves should be measured in an infinite field where the magnetization is directly parallel to the direction of the applied field. Usually the difference between high, practical fields and infinite fields is negligible; however, Kouvel and Graham[10] outline a clever method that permits extrapolation to infinite fields when it is not. This technique requires a large number of torque curves to be taken for increasing fields. For a more complete treatment the reader is referred to the original paper.

---

9) R. F. Pearson and L. Guilford, Report No. 2159, Mullard Research Laboratories, December, 1957.

10) J. S. Kouvel and C. D. Graham, Jr., "Conference on Magnetism and Magnetic Materials," AIEE, Publication T-91, February, 1957, p. 85.

## Applications of the Instrument

### Anisotropy Measurements

Thus far measurements have been made on several single crystals of synthetic magnetite ($Fe_3O_4$),* nickel, and yttrium iron garnet (all cubic).

One magnetite crystal was first measured in a (100) plane of an ellipsoidal sample ($V \cong 1.1 \times 10^{-2}$ cm$^3$; major axis about 4 mm). A second was ground into a sphere ($V \cong 4.4 \times 10^{-3}$ cm$^3$) and oriented in a (110) plane. A run from liquid-nitrogen to room temperature was taken of the latter. Figure 18

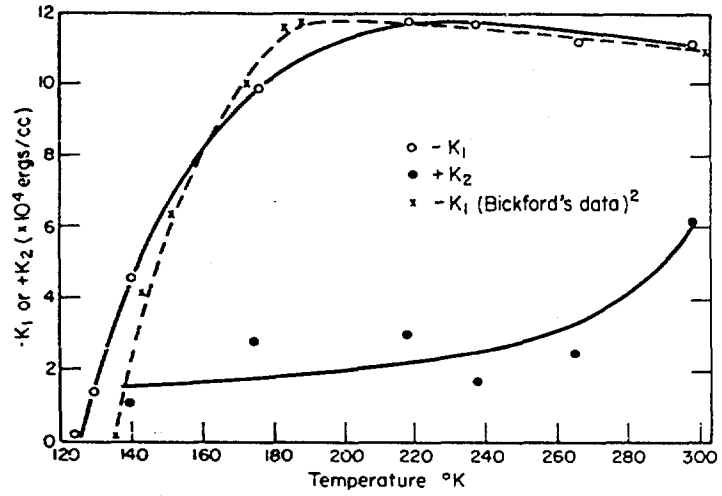


Fig. 18. $K_1$ or $K_2$ vs. temperature for magnetite.

shows the results along with points for $K_1$ taken by Bickford[2] in a resonance experiment. Room-temperature values are summarized in Table 3, The values of $K_1$ are generally consistent with those in the literature, which run from -0.98 to -1.20 x 10$^5$ ergs/cm$^3$.

A room-temperature measurement on a disk ($V \cong 6 \times 10^{-2}$ cm$^3$; r = 9 mm) of nickel† was run, giving values of $K_1$ = -50,000 and $K_2$ = 14,000 ergs/cm$^3$ at room temperature. A sample-torque curve is shown in Fig. 19. The value of

---

* Grown in the Laboratory for Insulation Research at M.I.T. by the Bridgman-Stockbarger method (cf. Tech. Rep. 49, December, 1951).

† Purchased from the Virginia Research Institute and made available by the Lincoln Laboratory of M.I.T.

$K_1$ compares favorably with -49,000, the average of ten values cited by Bozorth.[1] No reliable values of $K_2$ have been published.

Finally a temperature run on an yttrium iron garnet sphere* ($V \cong 4.2 \times 10^{-3}$ cm$^3$) was made with the results shown in Fig. 20 along with Dillon's[11] data.† The anisotropy differed in several of the (110) planes, indicating that the crystal was probably strained or contained some irregular-shaped impurities. A room-temperature measurement on a single-crystal disk with a greater volume ($V = 2.8 \times 10^{-2}$ cm$^3$) gave reasonable agreement with the previous results.

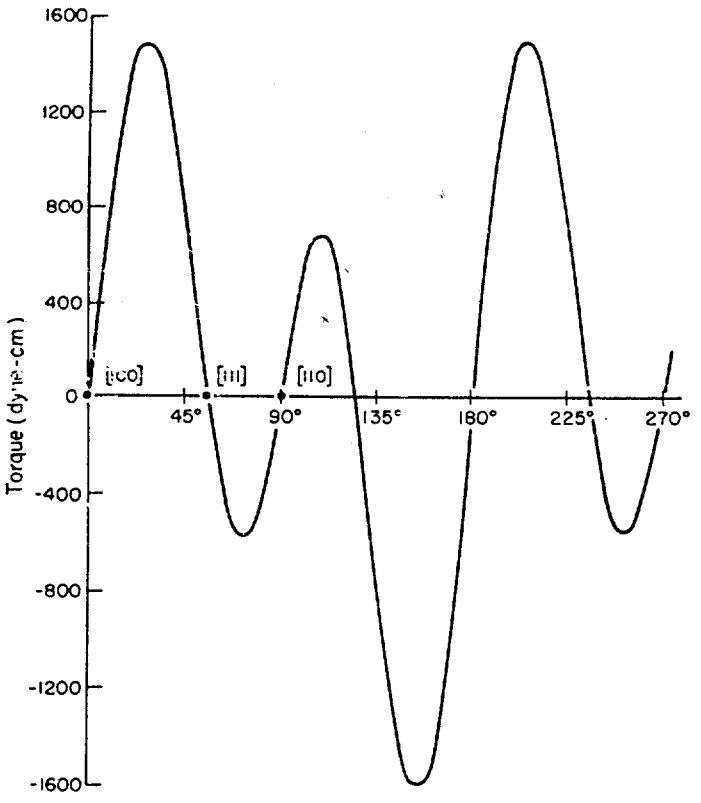


Fig. 19. Torque vs. angle curve for nickel in the (110) plane at 20°C.

Table 3. Room-temperature anisotropy constants (in ergs/cm$^3$).

| | $K_1$ | $K_2$ |
|---|---|---|
| Magnetite ellipsoid | $-1.13 \times 10^5$ | - |
| Magnetite sphere | $-1.12 \times 10^5$ | $(6 \pm 3) \times 10^4$ |
| Nickel disk | $-5.0 \times 10^4$ | $(1.4 \pm 0.5) \times 10^4$ |
| Yttrium iron garnet sphere | $-6.1 \times 10^3$ | $(1.0 \pm 0.5) \times 10^4$ |
| Yttrium iron garnet disk | $-6.5 \times 10^3$ | $(0.5 \pm 0.5) \times 10^4$ |

* Grown in a $PbO$-$PbF_2$ flux by a process similar to that described by Nielsen, Suppl. to J. Appl. Phys. 31, No. 5, 51S (1960). The sample was obtained from Air Force Cambridge Research Center.

11) J. F. Dillon, Phys. Rev. 105, 759 (1957).

† To find $K_1$ from Dillon's data given in terms of $K_1/M_s$, we used values of $M_s$ found by Pauthenet, J. Appl. Phys. 29, 253 (1958).

## Rotational Hysteresis

Since the torque magnetometer measures minute torques, it can also be used to study rotational hysteresis. If a sample is suspended in a uniform magnetic field and rotated in this field (or the field is rotated around it), the rotational hysteresis $W_r$ is defined as the energy loss per radian per unit volume:

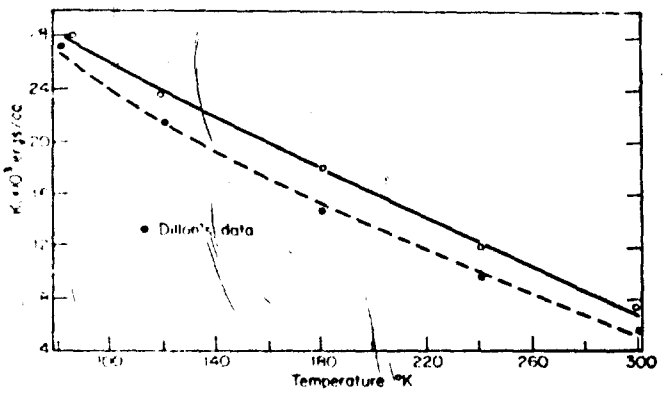


Fig. 20. $K_1$ vs. temperature for yttrium iron garnet.

$$W_r \triangleq -\frac{1}{2\pi V}\int_0^{2\pi} L(\theta)d\theta, \qquad (32)$$

where V is the volume of the sample and the torque is given in dyne-cm. The rotational hysteresis energy loss represents that amount of work that must be done on the crystal in order to rotate the magnetization through 1 radian. It usually appears in the crystal as thermal energy.

The rotational hysteresis of a polycrystalline yttrium iron disk sample as a function of the measuring field is shown in Fig. 21.

## Induced Anisotropy

In certain polycrystalline materials, such as yttrium iron or lutetium iron garnet, a uniaxial anisotropy may be annealed into the specimen by cooling in a large field. For polycrystalline YIG a uniaxial anisotropy of about 900 ergs/cm$^3$ was induced by annealing in a 6-kg field from room to liquid-nitrogen temperature. This represents

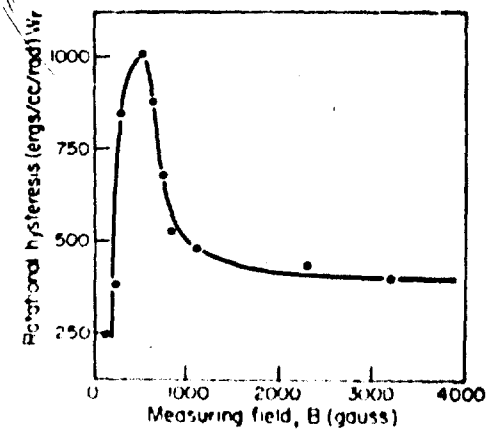


Fig. 21. Rotational hysteresis of polycrystalline yttrium iron disk.

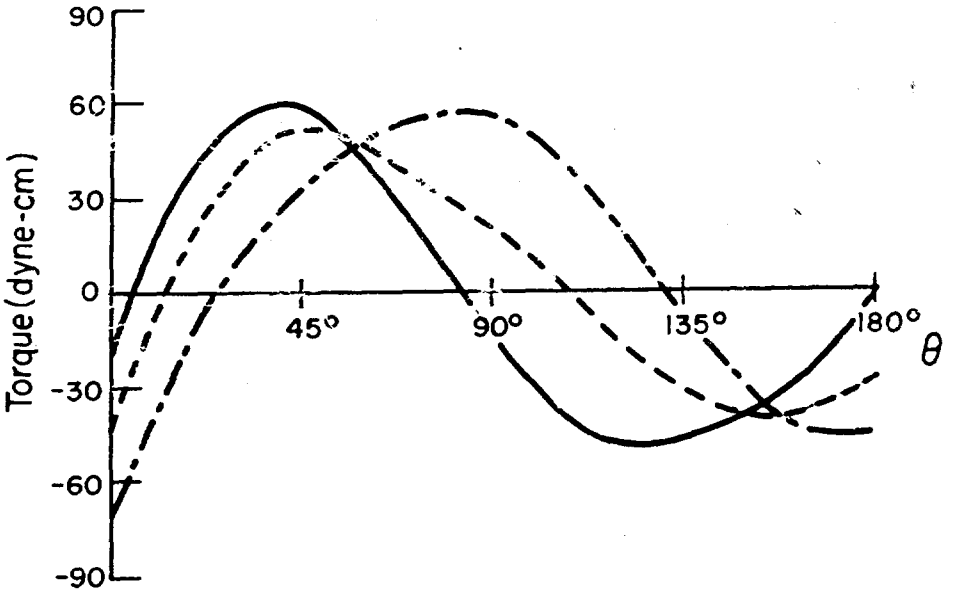


Fig. 22. Field-induced anisotropy in polycrystalline yttrium iron garnet.

roughly 5% of the single-crystal value. For LIG a value of about 3500 ergs/cm$^3$ (or 50% of the single-crystal value) was similarly obtained. By altering the direction of the applied field when at 77°K, the axis of symmetry can be rotated (Fig. 22).

Decay Mechanism

It has also been found that a relaxation process is associated with materials exhibiting the previous anneal effects that can be observed with the torque magnetometer. This may be seen by annealing the sample as before and subsequently altering the direction of the applied field by 45 degrees to coincide with the position of maximum torque as dictated by the uniaxial anisotropy. There will be a torque due to the "initial" anisotropy, which will decay with time approximately as an exponential as the easy direction of magnetization relaxes over to the new position. This relaxation process for YIG has a time constant of about 30 seconds (Fig. 23).

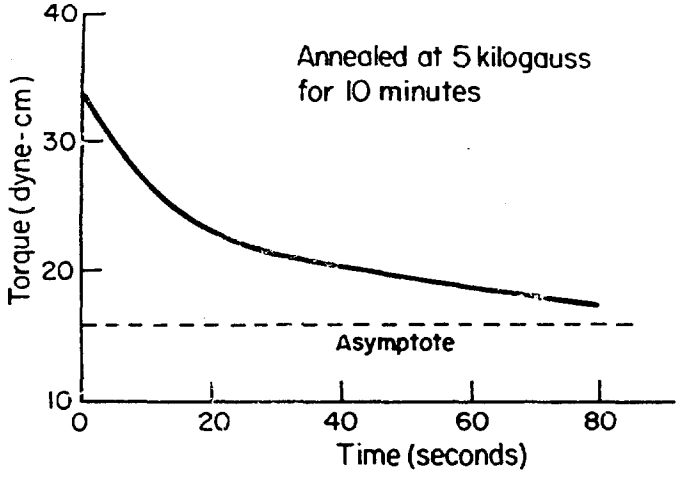


Fig. 23.

Torque relaxation curve for yttrium iron garnet.

## Conclusion

The torque magnetometer has been developed to the point where it may be used for routine measurements of magnetic anisotropy, rotational hysteresis, and anneal effects over a wide temperature range, to be ultimately extended to liquid helium.

## Acknowledgment

The author is indebted to the many members of the Laboratory for Insulation Research who offered their skillful assistance and advice throughout all phases of this project. In particular he would like to mention Professor D. J. Epstein and Mr. B. Frackiewicz for their many helpful suggestions and discussions.